Experimental study of forbidden optical transitions in a dense, laser-produced plasma*

R. J. Hawryluk, G. Bekefi, and E. V. George
Department of Physics and Research Laboratory of Electronics, Massachusetts Institute of Technology, Cambridge, Massachusetts 02139
(Received 17 January 1974)

The intensities and line profiles of several forbidden optical transitions, together with their companion allowed lines were measured in a helium plasma having densities N ranging between $\sim 1\times10^{16}$ and $\sim 5\times10^{16}$ cm^{-3}. The plasma was produced by irradiating helium gas with light from a repetitively pulsed, high-power CO_2 laser. The time and space-resolved spectra of three forbidden lines of He I were examined: the $2\,^1P$-$3\,^1P$ transition at 6632 Å, the $2\,^3P$-$4\,^3F$ transition at 4470 Å, and the $2\,^3P$-$4\,^3P$ transition at 4517 Å. The Abel-transformed line shapes were compared with recent theories and, while some discrepancies exist, their magnitude is considerably less than has been reported hitherto. A series of tests was made from which it is concluded that the existing disagreements are not the result of measuring deficiencies or errors in data processing, and are probably due to some remaining inadequacies of the theoretical models.

I. INTRODUCTION

It has long been known that the forbiddenness of an optical transition can be broken by a sufficiently strong external perturbation of the radiating (or absorbing) atom. Thus, the electric fields generated by the ion microfield[1] of a plasma, or turbulent plasma fluctuations,[2] will cause the emergence of forbidden optical transitions. An understanding of the intensities and shapes of these forbidden components relative to their companion allowed lines is desirable for several reasons. First, the lines appear in the spectra of early-type stars and thus figure importantly in model-atmosphere calculations.[3-5] Second, the intensities of forbidden lines are strongly dependent on the charged-particle density of the plasma, a fact which may well be exploited as a noninterfering diagnostic probe of dense, ionized media.[6] And third, detailed comparisons of the computed and measured line profiles provide a most sensitive test of modern line-broadening theories, the earliest of which are due to Griem,[7] Gieske and Griem,[8] Barnard, Cooper, and Shamey,[9] and Barnard and Cooper.[10] We note that these early theories are based on the traditional[11] model in which the sluggish ion motions are taken to be quasistatic and the electrons are treated in the impact approximation (any differences amongst the various formulations lie mainly in the way the electron broadening contribution is accounted for).

Comparisons of experiments with the aforementioned theories have disclosed notable disagreements[5,12-17]: the peak intensities of some measured forbidden lines (relative to the companion allowed lines) can be as much as a factor of 2 or more weaker, and the observed dips between the forbidden and allowed lines smaller, than theory would have it. In an attempt to account for these discrepancies, Burgess[18] suggested that the quasistatic ion approximation becomes invalid at and near the center of the forbidden line, a suggestion which Griem[19] and later Lee[20] placed on a more quantitative basis. While ion dynamics is now known to play an important role at the lower plasma densities ($N \lesssim 10^{15}$ cm^{-3}), and may well account for all the observed divergencies there, such cannot be the case at high densities. Computations show (see for example Ref. 16) that ion dynamic corrections become progressively smaller the large N, and when $N \gtrsim 10^{16}$ cm^{-3}, ion dynamics can no longer be invoked in all cases of observed discrepancies.

In this paper we limit ourselves to this latter regime of high plasma density ($10^{16} \lesssim N \lesssim 5\times10^{16}$ cm^{-3}) where unanswered problems remain. To this purpose we carry out a detailed examination of the following combination of allowed and forbidden lines:

for He I, $2\,^1P$-$3\,^1D$ at 6678 Å,
$2\,^1P$-$3\,^1P$ at 6632 Å;
for He I, $2\,^3P$-$4\,^3D$ at 4471.5 Å,
$2\,^3P$-$4\,^3F$ at 4470 Å,
$2\,^3P$-$4\,^3P$ at 4517 Å.

Comparison presented in Sec. III of the Abel-transformed line shape measurements with recent computations will show that while some discrep-

ancies still remain, their magnitude is considerably less than had been reported previously.[13,14,16] This reduction in the discrepancies is in part due to improvements in line shape measurements and data analysis, and in part due to better theoretical models.

In addition to the above-named overlapping lines we have also made extensive use of isolated lines which are relatively well understood theoretically. We have used such lines in diagnosing the plasma in regard to its spatial and temporal density and temperature distribution, and also for checking the optical setup and techniques of data reduction. This work is described in Sec. II.

II. PROPERTIES OF THE SPECTROSCOPIC SOURCE

A. Optical setup

The 10.6-μ infrared radiation from a very stable, repetitively pulsed CO_2 laser described earlier[21] was focused by a germanium lens into a helium cell provided with a salt window, which transmitted the laser pulses. The cell was evacuated to a pressure of 10^{-6} Torr and then filled with spectroscopic grade helium to a pressure of about $\frac{3}{4}$ atmosphere, before being sealed. The plasma was produced by optical breakdown at the focal spot of the lens. It was cigar-shaped with its major axis along the direction of the incident laser radiation. As shown in Fig. 1, the light from the plasma passed through a condensing lens, an optical flat and was focused onto the entrance slits of the spectrometer. The magnification of the lens system was 1.7. The lens was located 23.7 cm away from the spectrometer and 14.8 cm away from the plasma. Spatial resolution was about 0.01 cm using a slit height of about 0.02 cm. Scanning perpendicular to the major axis was achieved by manually rotating the thick flat optical plate. This focused different transverse positions onto the entrance slit of the spectrometer. The 0.5-m spectrometer (Jarrell-Ash model 82-020) was provided with a motor driven wavelength scan and a photomultiplier output. RCA 6199 and C31000 K photomultiplier tubes were used in our measurements. Their spectral responses (including that of the spectrometer itself) were determined by employing a subsidiary lamp with a tungsten ribbon filament whose emissivity was previously established.

The output from the photomultiplier tube was fed into a boxcar integrator (Princeton Applied Research model 160) and from there onto a strip-chart recorder. The gate width used on the boxcar integrator was 250 nsec and was the time resolution of the experiment. The delay could be set to any time after initiation of the laser pulse (in our final data, all the profiles were taken at 5 μsec in the afterglow of the plasma). A small fraction of the laser pulse was reflected out of the main beam by a salt flat and directed into a nitrogen cooled gold-doped germanium detector. Besides monitoring the laser power, the output of the detector was used to trigger the boxcar integrator and an oscilloscope which displayed the photomultiplier output and the gate on the boxcar

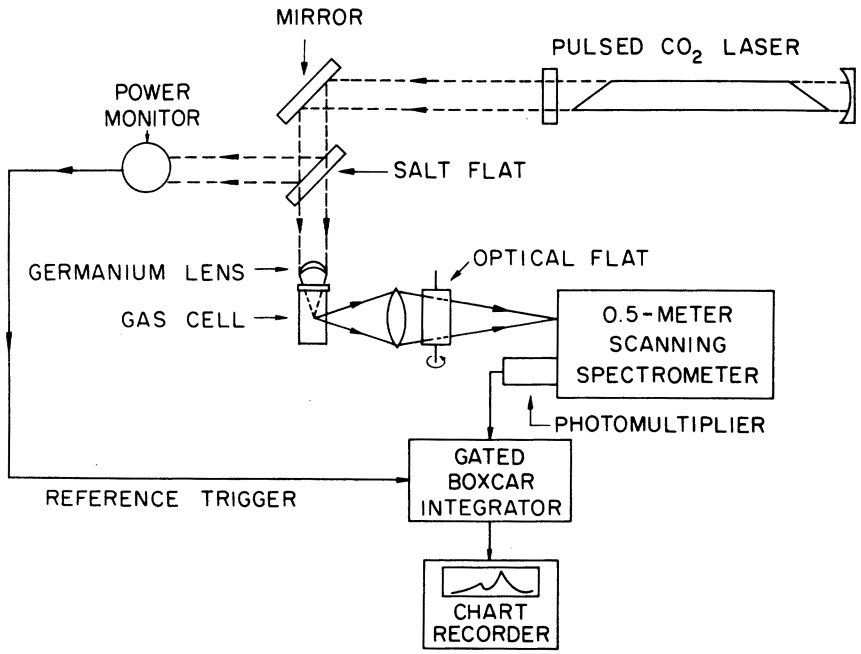

FIG. 1. Schematic diagram of the experimental setup.

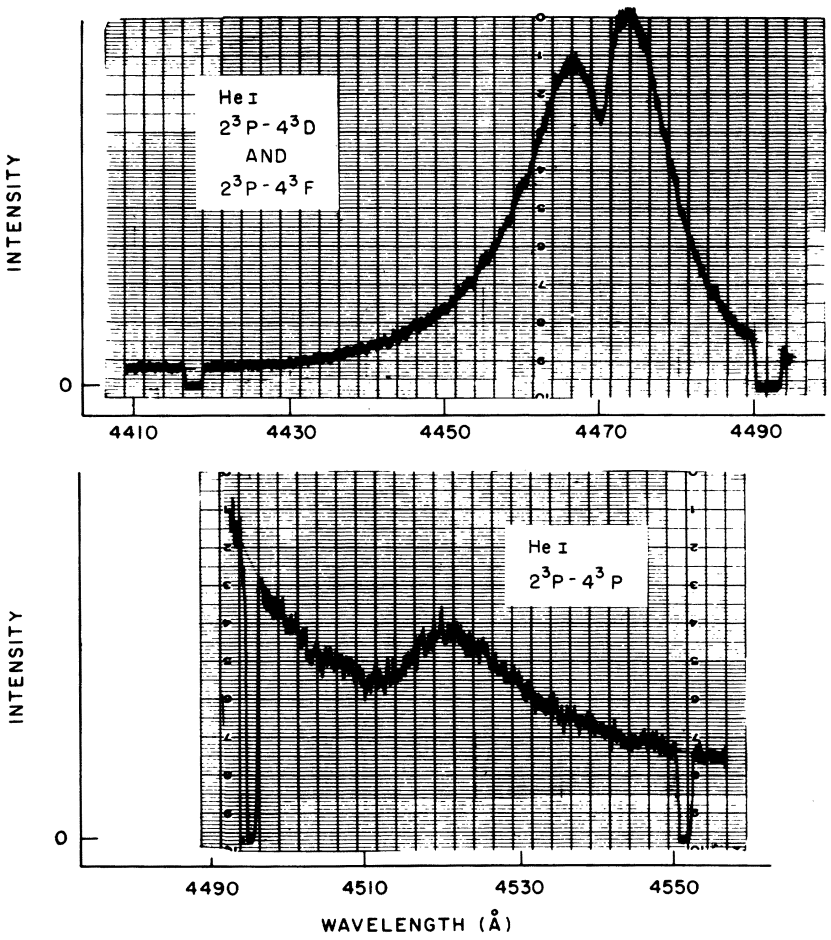

FIG. 2. The measured intensity profiles of the allowed He I 4471-Å line and the forbidden He I 4470-Å line (top), and the forbidden He I 4517-Å line (bottom). The peak intensity of the distant forbidden line shown is $\sim\frac{1}{20}$th that of the allowed line.

integrator. Thus, the sweep on the boxcar integrator and the oscilloscope were directly referenced to the laser pulse through the detector. One reason for this elaborate triggering mechanism was that the spectrometer, the optical flat, the condensing lens, and all the electronic equipment with the exception of the CO_2 laser and its power supply were housed in a large screened box. This eliminated electrical pickup from the laser discharge and further increased the signal-to-noise ratio. Figure 2 illustrates the kind of signal-to-noise ratios encountered while measuring some strong allowed lines and weak forbidden components. Signals as low as 35 dB below the peak signal of a fairly strong allowed line could be measured with reasonable accuracy. The good short and long range stability of the laser output and its fast repetition rate (12 pulses per second) permitted rapid gathering of spectroscopic data. For example, the line shapes shown in Fig. 2 were obtained in about 45 min running time.

The thick optical plate (see Fig. 1) located between the condensing lens and the spectrometer was mounted in a holder which was capable of being rotated about its axis by means of a micrometer shaft. To calibrate the readings of the micrometer in terms of the true image displacements (here called the y positions) we used inverse optics and proceeded as follows. A mercury discharge tube was placed at the exit slits of the spectrometer. The mercury light emerged from the spectrometer through the optical plate and was focused into a mockup cell replacing the actual helium cell. The mockup cell was a half of a Pyrex tube having the same diameter as the helium cell and cut along its major axis. Hence, the light was refracted through the mockup cell, just as it would have been through the helium cell used in the experiments. The condensing lens focused the light into the cell. A second lens was used to increase the magnification, and the final image was projected onto a screen where its position could be determined very precisely. Knowing the focal length of this lens and the screen's distance from it, the desired calibrations of the "y positions" of the image in terms of the micrometerhead rotations were de-

duced. Image displacements with errors smaller than 0.005 cm were thus achieved. Note that at the time of measurement (5 μsec in the afterglow) the plasma was only ~0.4 cm in lateral size, and very small image displacements were therefore desired. While performing the foregoing calibration, we observed that the image on the screen suffered from aberrations which increased with plate rotation. However, for the small rotations used during actual experimentation, the image distortions proved to be quite negligible.

B. Abel inversion

Our laser produced plasma "cylinder" has pronounced radial density and temperature gradients. For that reason the light intensity $I(y,\lambda)$ measured at a given wavelength λ, and integrated over a given cord displaced a distance y from the axis of the plasma cylinder, must be Abel-inverted[22] to yield the "true" line profile as specified by the local emission coefficient $\epsilon(r,\lambda)$ (instrumental line broadening was negligible in all our measurements). To this purpose a series of profiles like those illustrated in Fig. 2 was taken at some 20–30 different lateral positions y covering the entire dimension of the plasma (~4 mm). Each measured profile was then digitalized into ~50 wavelength intervals and the approximately 1500 data points of $I(y,\lambda)$ were fed into a computer code which performed the Abel-transform, yielding $\epsilon(r,\lambda)$ for the line contour in question. However, before this task was undertaken, we had to assure ourselves of the following prerequisites upon which an Abel-inversion is based: (i) that the observed light rays be virtually paraxial; (ii) that the plasma be optically thin; (iii) and that it be cylindrically symmetric. We shall now address ourselves to these points.

(i) *Paraxial rays.* In order to evaluate to what extent the paraxial ray assumption is met in our experimental arrangement, an aperture of variable size was placed at the lens assembly as is shown at the top of Fig. 3. The size of apertures chosen was 1 cm in diameter, 2 cm in diameter, and no aperture so that in the last case the full size of the condensing lens (6.3 cm) was exposed. Thus, the solid angle θ subtended by the apertures (see Fig. 3) was varied by a factor ~40. The He 4471-Å-line and its forbidden component were now studied at various locations y from the plasma axis as a function of aperture size. The ratio I_2/I_1 of the peak intensity of the forbidden line to the allowed line, and the distance $\Delta\lambda$ between the forbidden and the allowed lines were measured and tabulated. These characteristic quantities are sensitively dependent upon the plasma density; thus, if the line profiles change as a function of

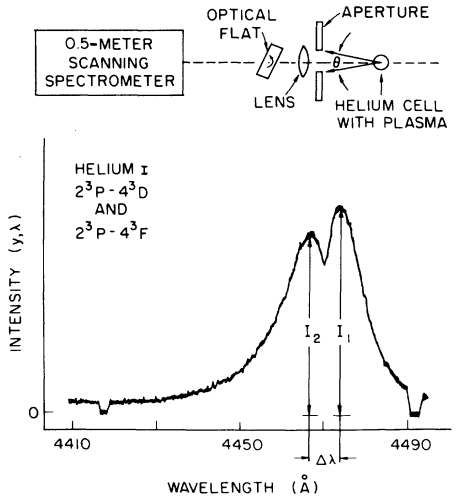

FIG. 3. Experiment used to test the paraxial ray assumption. The line profile shown is that of the He I 4471-Å line and its forbidden component. I_1 is the intensity of the peak of the allowed line and I_2 is the intensity of the peak of the forbidden line. The wavelength separation between the allowed and forbidden lines is $\Delta\lambda$.

the aperture size, the rays entering the spectrometer cannot be considered paraxial. Table I shows that within the reproducibility of the data no significant or systematic effects of varying the aperture size occur. A study of the depth of the dip between the forbidden and allowed lines is likewise uneffected by changing apertures.

(ii) *Self-absorption.* Since the Abel inversion assumes that the plasma is optically thin, a series of experiments was conducted to measure the extent of self-absorption. An 8-cm focal length spherical mirror was placed 16 cm behind the center of the plasma. The light emitted by the plasma away from the spectrometer was reflected by the mirror back into the plasma and then via our condensing lens, onto the spectrometer slit. The solid angle subtended by the mirror was chosen to match the solid angle subtended by the condensing lens. The peak intensity of a given line was measured and compared with the peak intensity obtained in the absence of the spherical mirror. From this the effective absorptivity of the plasma fireball could be determined. The results are shown in Table II for several lines of interest, measured at various times in the afterglow.

Table II indicates that early in the afterglow most lines suffer from substantial self-absorption. Our choice of 5 μsec for all our line shape studies was motivated by this fact; at still later times, of course, the plasma density falls to too low a level. We note that even at 5 μsec some self-

TABLE I. Effect of a limiting aperture on the profile of the HeI 4471-Å line and its forbidden component at 4470 Å (see Fig. 3 and text for explanation of symbols).

Distance y from plasma axis (mm)	Aperture diam (cm)	Intensity ratio I_2/I_1	Wavelength separation $\Delta\lambda$ (Å)
0.0	1.0	0.797	5.80
0.0	2.0	0.792	5.80
0.0	6.3	0.797	5.55
1.44	1.0	0.507	3.20
1.44	2.0	0.543	3.25
1.44	6.3	0.480	3.20

absorption occurs. The important He I 6678-Å line has an $A \approx 0.2$ and one thus expects that an error of about 20% will occur at the line center. We note here however, that our method of analyzing the data and comparing them with theory is not affected by the mild self-absorption at the line center. The He I 5876-Å line, on the other hand is heavily self-absorbed and is inappropriate for line shape studies. We have used it merely in determining the electron temperature from the integrated intensity ratio of the He II 4686-Å-line to the He I 5876-Å line. This ratio is relatively insensitive to quite large errors in the intensity of the He I 5876-Å line, as will be discussed later.

(iii) *Symmetry*. If the mirror which deflects the laser beam into the germanium lens as shown in Fig. 1 is not carefully positioned with respect to the germanium lens, the plasma loses its cylindrical symmetry. Therefore, before each set of line shape measurements, the symmetry was checked by measuring $I(y, \lambda)$ for a number of y positions and repeating this procedure for slightly different mirror adjustments, until a good cylindrically symmetric plasma was obtained. Despite all reasonable precautions however, an analysis of our final data showed small, 10% at worst, asymmetries. The effect of the asymmetries was to make measurements of the He I lines near the plasma core somewhat unreliable. Thus, all He I line profiles used for comparison with theory were taken from the cool outer halo, where the emissivity $\epsilon(r, \lambda)$ as a function of radius r was less prone to error in the Abel-inversion. Here also the gradients of charged particle density and temperature were not too severe (see Figs. 6 and 7) and the concentration of excited neutral atoms large—facts which make for additional reliability of the data analysis.

We have shown that the criteria for a good Abel-inversion have been met very well. This is further confirmed in the next subsection where we make several comparisons between theory and measurements of contours of certain isolated lines.

C. Stark broadening of isolated allowed lines

The Stark-broadened line shapes of isolated helium transitions are well understood theoretically.[23-25] Thus, a comparison of measured line shapes with computed ones, serves as an additional check on the quality of the optical system and on Abel-inversion techniques. In any such comparison one must subtract from the measured intensity the underlying continuum and one must also choose a factor which normalizes the theoretical line shape to the experimentally determined $\epsilon(r, \lambda)$

TABLE II. Self-absorption of different spectral lines of helium at different times in the plasma afterglow. (The plasma is optically transparent when A is zero and fully self-absorbing when A is unity.)

Spectral line (Å)	Time in afterglow (μsec)	Absorptivity A
HeI 6678	0.5	0.40
	2.0	0.10
	5.0	0.23
	8.0	0.31
HeI 5876	0.5	0.43
	2.0	0.61
	5.0	0.67
	8.0	0.71
HeI 4713	0.5	0.69
	2.0	0.04
	5.0	0.04
	8.0	0.00
HeII 4685	0.5	0.04
	2.0	0.02
	5.0	0.07
HeI 4471	0.5	0.52
	2.0	0.04
	5.0	0.01
	8.0	0.02
HeI 4470	0.5	0.52
	2.0	0.12
	5.0	0.07
	8.0	0.04

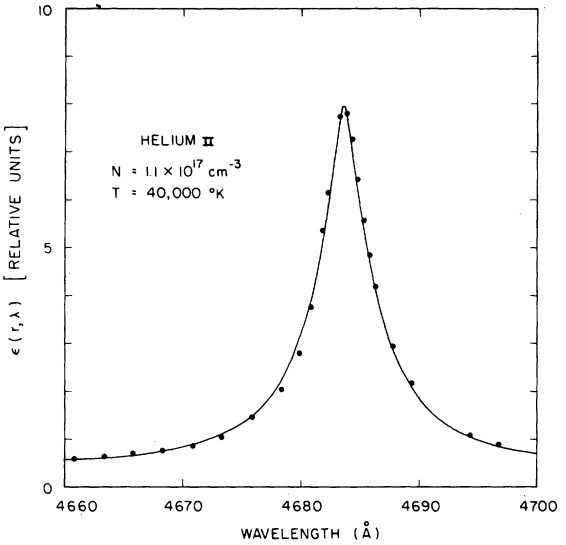

FIG. 4. Stark-broadened profile of the He II 4686-Å line. The dots represent the Abel-inverted experimental profile and the solid line represents the theoretical profile with $N = 1.5 \times 10^{17}$ cm^{-3} and $T = 40\,000$ °K.

(which is usually known only as readings in some relative units). An unequivocal experimental determination of the continuum is usually very difficult, requiring large wavelength excursions from the line center. Here the signal-to-noise ratio can be poor, and neighboring lines may well mar such a measurement. For that reason the continuum level and the normalization constant are customarily treated as adjustable parameters and we shall treat them that way here.

Figure 4 shows a comparison between experimental and theoretical contours of the He II 4686-Å line. The computed profile was obtained from tabulated values.[26] The agreement is seen to be good. Figure 5 shows a typical profile of the He I 4713-Å line. The solid line refers to the fitted theoretical profile based on a computer program supplied by Ya'akobi and Griem.[27] The small but unmistakable discrepancies between the measured and theoretical line shapes are not understood; they are similar to the discrepancies reported by earlier workers[23] and for that reason we feel that they are not caused by instrumental effects.

D. Density and temperature measurements

At the instant of creation, the laser-produced plasma fireball has an electron density approaching[28] 10^{19} cm^{-3} and a temperature several tens of electron volts. The plasma is then expanding[21] with a velocity of about 2×10^5 cm/sec. At a time of a few hundred nanoseconds into the afterglow the expansion slows down perceptibly and the plasma becomes sharply differentiated into a dense hot inner core which is almost at a standstill, and a slowly expanding, relatively cool and tenuous halo. This sequence of events is similar to the time history of a blast wave generated during strong explosions,[29,30] where initially the luminous fireball and shock front expand together as one unit. Eventually however, the shock front cools sufficiently and loses much of its luminosity. At this time the shock breaks away and leaves the now slowly expanding luminous fireball far behind. At 5 μsec in the afterglow, the time at which the data presented in this paper were measured, the laser generated plasma has virtually ceased expanding.[21] The radius of the cigar shaped plasma at this time is about 2 mm and its length 6–10 mm. It is composed of a dense, hot inner core and a cool outer halo.[21] To diagnose these two vastly different regions, different spectroscopic lines were used.

In the core region, the radial distribution of plasma density was deduced from the width[26] of the Stark-broadened He II 4686-Å line, which was appropriately Abel-transformed as described in

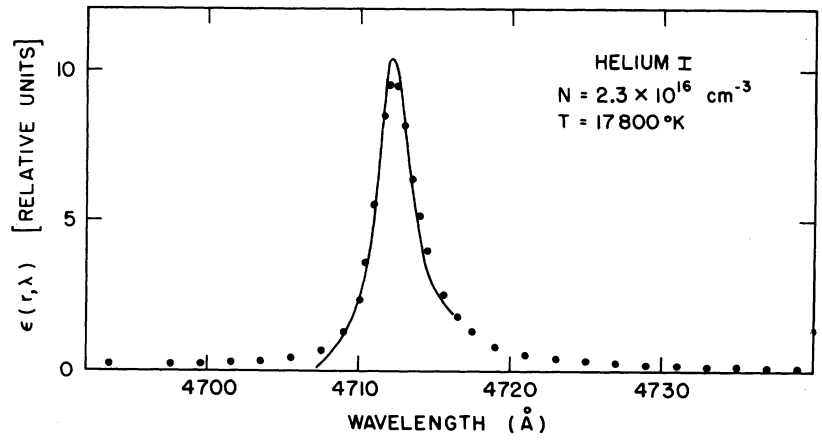

FIG. 5. Stark-broadened profile of the He I 4713-Å line. The dots represent the Abel-inverted experimental profile and the solid line represents the best fit theoretical profile with $N = 2.3 \times 10^{16}$ cm^{-3} and $T = 17\,800$ °K.

Sec. IIB above. The electron temperature in the core was derived from the ratio of the integrated intensity of the He II 4686-Å line to the integrated intensity of the He I 5876-Å line using the tabulated results of Mewe.[31] There are several sources of error in this measurement. First, as pointed out before, the He 5876-Å line was significantly self-absorbed. Secondly, and more importantly, the He 5876-Å line shape is suspect in the core. For radial positions near the center, the Abel-inversion is very sensitive to experimental error. Because the plasma is hotter and more dense in the center, the density of neutrals is less than in the halo. Between small plasma asymmetries, mentioned earlier, and errors in measuring the data, the Abel-transform can give erroneous results. Third, there are small errors from the system response calibration. Fortunately, the plasma temperature is fairly insensitive to errors in the integrated intensity ratio of He II to He I. Suppose that the intensity ratio is unknown to within a factor of 10. From Mewe's data[31] (for a density of 1.28×10^{17} cm^{-3} and a temperature around 4.0 eV) factors of 10 in the intensity ratio above and below the 4-eV point result in temperature spread which extends from 4.7 to 3.6-eV corresponding to +19% and −14% errors, respectively. The intensity ratios in our measurements are known much better than this.

In the halo, the density was determined by fitting the entire measured (and Abel-transformed) He I 4713-Å profile to a computer generated theoretical profile.[27] The temperature in the halo was determined from the ratio[11] of the integrated line intensity to the integrated continuum intensity in a 100-Å band centered around the He 6678-Å line and around the He 4713-Å line. The value of the continuum for the He 6678-Å line was obtained in the vicinity of the forbidden line near 6588 Å. The value of the continuum for the He 4713-Å line was obtained in the red wing of the line (away from the He I 4686-Å line whose intensity is anyway negligible at these radial positions in the halo).

The radial density and temperature distributions derived from the above measurements are shown in Figs. 6 and 7, respectively. We note that both N and T exhibit almost discontinuous jumps at a radial position $r\simeq0.9$ mm, which delineates the hot dense inner core from the cool halo. Earlier studies[21] showed the existence of the discontinuity in N but not in T. The present measurements are both more extensive and more reliable. We believe using very conservative estimates, that the values of $N(r)$ are accurate to better than ±15% and those of $T(r)$ to better than ±25%.

In measuring the density distribution $N(r)$ we attempted to obtain some experimental points across the "density jump." We first tried to extend the He II 4686-Å line width measurements to larger radial distance than shown in Fig. 6.

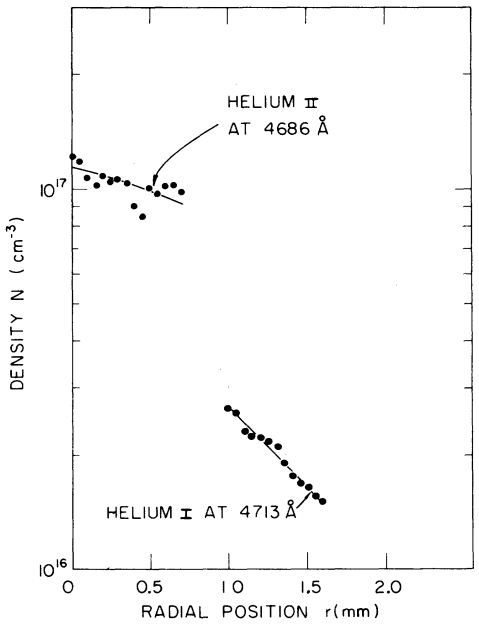

FIG. 6. Density of the plasma as a function of radial position, obtained from the He I 4713-Å and the He II 4686-Å spectral lines.

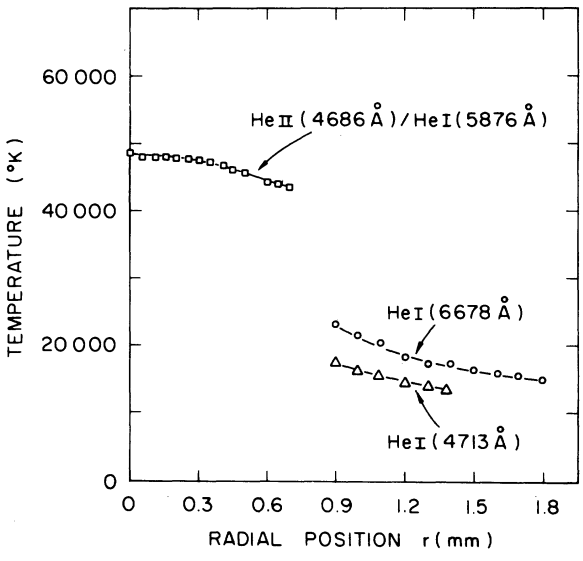

FIG. 7. Temperature of the plasma as a function of radial position, obtained from the integrated intensity ratio of the He II 4686-Å line to the He I 5876 line and from the line to the continuum ratio of the He I 6678-Å line and for the He I 4713-Å line.

We failed because the absolute light intensity of the 4686-Å line falls rapidly across the discontinuity and this makes it virtually impossible to obtain a line profile (for example, when r is varied from 0.75 to 1.0 mm, the integrated line intensity diminishes by two orders in magnitude). Linewidth measurements of the He I 4713-Å line across the discontinuity were then carried out and the results Abel-transformed. The results proved neither reliable nor reproducible and are therefore not presented in the figure. The cause for the poor quality of the data is ascribed to slight asymmetries of the plasma and to density gradients of the neutral particle distribution, as discussed already in (iii), Sec. IIB, above. We wish to point out that recent independent measurement of $N(r)$, using laser interferometry,[28] exhibit pronounced radial density gradients similar to ours and thus tend to substantiate our observations. The observed density discontinuities were less pronounced than ours, mainly because the measurements were made at ~300 nsec in the afterglow, at a time when the plasma has as yet not fully differentiated into the two regimes of core and halo. The electron temperature distribution of Fig. 7 likewise shows a sharp change at the core-halo boundary. And, just as in the density determinations, the He I and He II spectroscopic observations could not be extended beyond the radial positions shown. Note that the temperature determinations using He I 4713-Å differ by about 25% from those made with He I 6678 Å. This discrepancy has as yet not been explained satisfactorily.

When the laser power level is increased somewhat, the results of Figs. 6 and 7 remain qualitatively the same. All that is observed is a slight increase in plasma density and temperature. The studies on forbidden lines discussed in Sec. III below were made with two slightly different power levels. Specifically, the measurements shown in Figs. 8 and 9 were carried out at higher powers than the remaining measurements. In *all* cases, however, the observations were made well within the plasma halo (away from the core-halo boundary), where N and T show relatively mild variations with radius.

III. FORBIDDEN LINES

A. He I $2\,^3P$-$4\,^3F$ line

The top of Fig. 2 illustrates a typical recorder output of the $2\,^3P$-$4\,^3F$ forbidden line almost completely merged (at these densities) with the neighboring $2\,^3P$-$4\,^3D$ allowed component. This plot refers to the case when the spectrometer looks directly towards the plasma center ($y=0$). Data like that shown in Fig. 2 were obtained for some 20 lateral y positions and the results Abel-transformed. The experimental results for a single radial position in the plasma halo are shown in Fig. 8 as solid dots.

In comparing the measurements with theory, the underlying continuum, treated as an adjustable parameter, was subtracted out. The dashed line represents the theoretical profile computed by the same methods as employed earlier by Griem.[7] The solid line refers to recent calculations by Deutsch *et al.*[32] in which the electron collision operator, which accounts for electron broadening, has been treated on a much more rigorous basis. In addition, these authors included a part of the ion dynamics through dynamic shielding of the ion-ion correlation, thus causing an enhancement of the low frequency part of the microfield distribution.

We see that our measurements agree better with the theory of Deutsch *et al.* than with those of Griem. Nonetheless, we observe discrepancies similar, but far less pronounced, to those re-

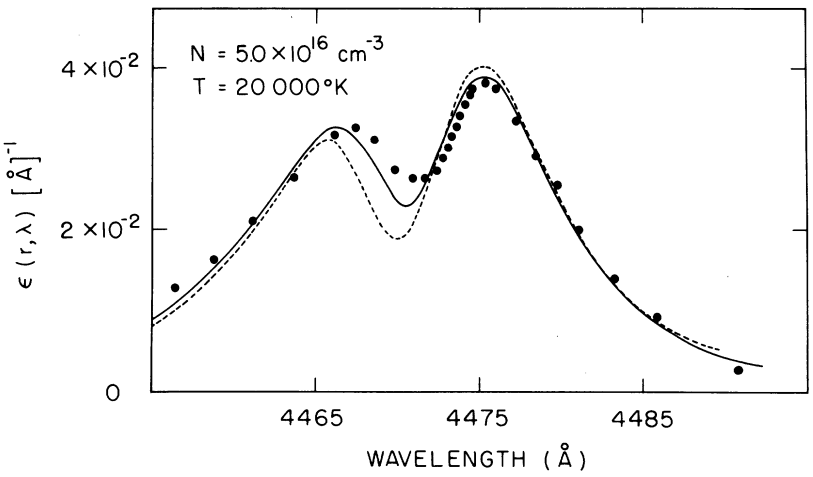

FIG. 8. Profiles of the allowed $2\,^3P$-$4\,^3D$ and the forbidden $2\,^3P$-$4\,^3F$ transitions. The dots denote the Abel-inverted experimental profile. The solid line represents the theory of Deutsch *et al.* (Ref. 32), and the dotted line represents the theory of Griem (Ref. 7) for $N=5\times10^{16}$ cm^{-3} and $T=20\,000$ °K.

ported earlier by Nelson and Barnard.[13] Whereas the overall half-width of the pair of lines agrees well with theory as do the distant blue and red wings, the detailed structure does not; the observed dip between the two lines is shallower than predicted by theory. It is clear that by merely changing the plasma density in the theoretical profile cannot lead to better agreement. For example, lowering the density makes the total half-width too small and the ratio of peak intensities even larger. It may be thought that the intensity ratio of the peaks is modified by self-absorption and that the filling in of the dip between the peaks is caused by an outer plasma region of relatively low density. We can refute self-absorption as a cause of error, since our measurements show that this is negligible at the time of measurement (see Table II). Also, line shape errors caused by density gradients should not be a problem, since the Abel-transformation of our results effectively corrects for the presence of gradients. It could be argued that forbidden lines are particularly sensitive to density gradient effects and that therefore an incomplete Abel-transform could be the cause of the errors. However, let us note that the distant forbidden line at 4517 Å is in good agreement with theory both in regard to its shape and its intensity relative to the allowed line (see below). Deutsch *et al.*[32] show that the dip between the allowed and forbidden lines is fairly sensitive to temperature, it being shallower the lower the temperature. In view of the likely inaccuracies in our temperature determinations, it may well be that at least some of the remaining discrepancy in the well-depth is due to a poor knowledge of the plasma temperature. Unfortunately we have at present no better way of determining T.

Recently, Jenkins and Burgess[14] have published a comprehensive experimental study of allowed and forbidden lines in helium plasmas of densities $\sim 1\times10^{16}$ to $\sim 3\times10^{16}$ cm^{-3}. Their disagreement with theory near the forbidden 4470-Å line is even more dramatic than that of Barnard and Nelson. Their profile (strongly convolved with an instrumental profile of sizable width) exhibits a virtual absence of a distinct peak at the forbidden position, and moreover the intensity in the measured blue wing is too low compared with theory. The authors speculate that weak plasma inhomogeneities may in fact be in large part responsible for the observed phenomena.

Figure 8 shows that the measured wavelength separation between the forbidden and allowed lines is somewhat smaller (by ~1 Å) than is predicted by theory. Previous observers[13,14] have seen the same effect. In our case, part (at most 0.4 Å), but not all of this discrepancy may be due to a systematic error in the wavelength calibration (the spectrometer exhibits an error of ±1 Å with periodicity of ~35 Å). The remainder appears to be a genuine discrepancy in the position of the forbidden line relative to the allowed component. To facilitate comparisons with various theories, Table III presents our measured line profile data. We note that the *absolute* values of the wavelengths given in the Table can be in error by as much as ±1 Å; the relative values, however, are of much greater precision.

The general picture which emerges from these comparisons suggests that existing theory satisfactorily explains the over-all width of the lines and their far wings, but that it fails mainly in the details near the peak of the forbidden line. Line-shape measurements made by us also at a lower density ($N \simeq 3\times10^{16}$ cm^{-3}) confirm the above results. The extraordinarily large discrepancies seen in Refs. 13 and 14, but not by us and by Birkeland *et al.*[15] do not seem to be genuine.

B. He I $2\,^3P$-$4\,^3P$ line

The detailed structure of the distant $2\,^3P$-$4\,^3P$ forbidden line is shown in Fig. 9. The solid dots refer to the Abel-transformed measurements and

TABLE III. Measured intensity profile of the He I 4471-Å line and of its two forbidden components at 4470 Å and 4515 Å. $N = 5\times10^{16}$ cm^{-3} and $T = 20\,000$ °K. The Abel-transformed line intensity is in relative units and includes the underlying continuum.

Wavelength (Å)	Intensity	Wavelength (Å)	Intensity
4455.0	16.5	4478.8	32.9
4457.5	21.5	4480.0	26.0
4460.0	27.3	4482.5	18.3
4462.5	34.6	4485.0	12.5
4465.0	42.0	4490.0	6.2
4466.3	43.1		
4467.5	41.0	4505.0	2.70
4468.8	36.4	4510.0	2.43
4469.4	34.8	4512.5	2.38
4470.0	34.9	4515.0	2.50
4470.3	36.7	4516.3	2.60
4470.6	34.6	4517.5	2.79
4470.9	35.3	4518.8	3.13
4471.3	36.3	4520.0	3.33
4471.6	37.5	4521.3	3.20
4471.9	38.5	4522.5	2.95
4472.2	41.3	4525.0	2.79
4472.5	43.3	4527.5	2.44
4473.1	45.9	4530.0	2.21
4473.8	49.5	4535.0	1.79
4475.0	50.0	4540.0	1.31
4476.3	43.8	4550.0	1.18
4477.5	38.7		

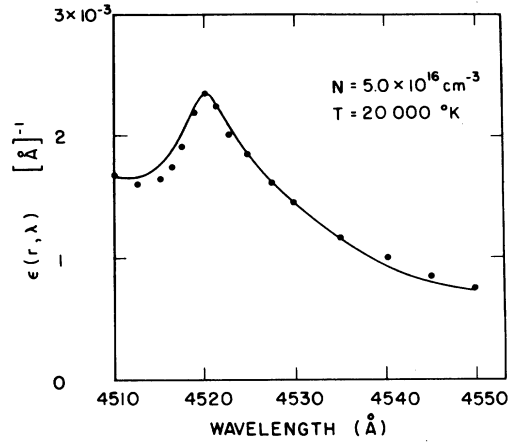

FIG. 9. Profile of the forbidden $2\,^3P$-$4\,^3P$ transition. The dots denote the Abel-inverted experimental profile and the solid line represents the theory of Griem (Ref. 7) for $N = 5\times10^{16}$ cm^{-3} and $T = 20\,000$ °K.

the solid line is the theoretical profile computed on the basis of Griem's[7] prescription. Note that we normalized the theory to the experiment at one point only, the peak of the companion allowed $2\,^3P$-$4\,^3D$ line, thus letting the peak of the forbidden line fall where it may. The agreement between measurements and theory is very satisfactory both in regard to the line shape and in regard to the peak height. A similarly good agreement has been obtained at a density $N = 3\times10^{16}$ cm^{-3}. This suggests that the $2\,^3P$-$4\,^3P$ line may well be exploited as a diagnostic tool in the determination of plasma densities in the range $N \gtrsim 10^{16}$ cm^{-3}.

C. He I $2\,^1P$-$3\,^1P$ line

Our most thorough measurements were made on the He I $2\,^1P$-$3\,^1P$ forbidden line at 6632-Å and its companion $2\,^1P$-$3\,^1D$ allowed transition at 6678 Å. An earlier,[16] less accurate version of these measurements, with poorer signal-to-noise, fewer y position measurements, and poorer data analysis, was presented in a previous publication. There we noted three major disagreements between experiment and the Griem theoretical prescription. (i) The peak of the forbidden line (relative to the allowed line) was about a factor of 2 lower than theory would have it. (ii) The measured dip between the two lines was too shallow by something like a factor of 2. (iii) The measured blue wing of the forbidden line fell off much too rapidly, yielding too low a total forbidden line intensity. We attempted to explain (i) and (ii) by the inclusion of ion dynamics; discrepancy (iii), on the other hand, remained unexplained.

New measurements and new data analysis, particularly in regard to the treatment of the underlying continuum which had previously been overestimated by us, disclose that while discrepancies (i) and (ii) remain in full force, discrepancy (iii) was not completely genuine. The solid dots of Fig. 10 show our new Abel-transformed measurements and Table IV gives the results in tabulated form. The solid line refers to the line shape derived[16] using the Griem prescription. In fitting the experiments to the theory we proceeded as follows. We computed the line profile for the value of N and T appropriate to the chosen radial position r in the plasma; we then treated the underlying experimentally observed continuum as an adjustable parameter, and by iterating N somewhat about the measured value, we fitted the red wing of the allowed line as best we could (no fitting was done at the peak of the allowed line in order to prevent errors caused by self-absorption, as discussed in Sec. II B). This fitting procedure leads precisely to the discrepancies (i) and (ii) discussed

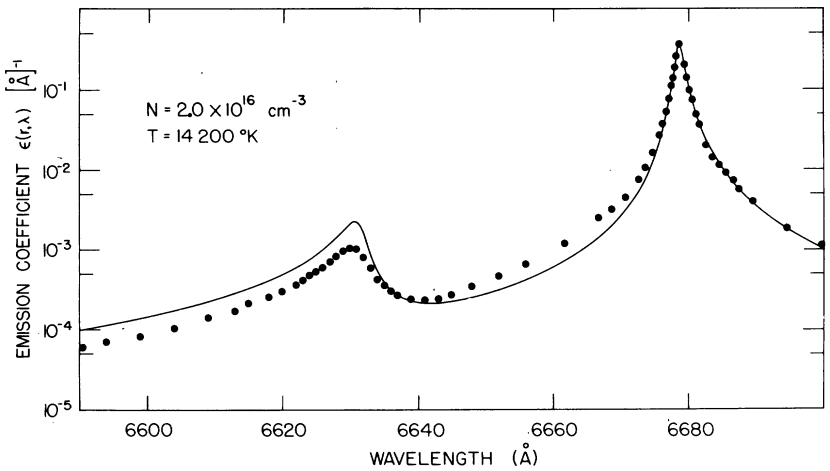

FIG. 10. Profiles of the allowed $2\,^1P$-$3\,^1D$ and the forbidden $2\,^1P$-$3\,^1P$ transitions. The dots represent the Abel-inverted experimental profile. The normalization factor and continuum level are so chosen as to give the best fit in the vicinity of the allowed theoretical profile obtained following Griem's approach. Note the discrepancies in the vicinity of the forbidden line.

TABLE IV. Measured intensity profile of the HeI 6678-A line and of its nearby forbidden component at 6632 Å. $N = 2\times10^{16}$ cm^{-3} and $T = 14\,200$ °K. The Abel-transformed line intensity is in relative units and includes the underlying continuum.

Wavelength (Å)	Intensity	Wavelength (Å)	Intensity	Wavelength (Å)	Intensity
6582.3	0.00491	6633.3	0.00996	6676.2	3.28
6587.3	0.00496	6634.3	0.00913	6676.4	4.57
6592.3	0.00515	6635.3	0.00859	6676.6	5.72
6597.3	0.00536	6637.3	0.00813	6676.8	6.34
6602.3	0.00569	6639.3	0.00798	6677.0	5.78
6607.3	0.00644	6641.3	0.00815	6677.2	4.90
6611.3	0.00690	6643.3	0.00863	6677.4	4.14
6614.3	0.00760	6646.3	0.00988	6677.6	3.57
6616.3	0.00832	6650.3	0.0119	6678.0	2.47
6618.3	0.00919	6654.3	0.0151	6678.4	1.74
6620.3	0.01032	6660.0	0.0245	6678.8	1.34
6621.3	0.0112	6665.0	0.0467	6679.4	0.88
6622.3	0.0122	6667.0	0.0590	6680.0	0.68
6623.3	0.0131	6669.0	0.0818	6681.0	0.40
6624.3	0.0143	6671.0	0.132	6682.0	0.257
6625.3	0.0161	6672.0	0.185	6683.0	0.210
6626.3	0.0182	6673.0	0.287	6684.0	0.167
6627.3	0.0206	6674.0	0.474	6685.0	0.135
6628.3	0.0220	6674.5	0.666	6688.0	0.077
6629.3	0.0214	6675.0	0.942	6693.0	0.038
6630.3	0.0179	6675.4	1.34	6698.0	0.0243
6631.3	0.0139	6675.8	1.98		
6632.3	0.0114	6676.0	2.44		

above, and to a slight discrepancy similar to that described under (iii). It is important to point out that there is no way of eliminating (iii) without introducing disagreement elsewhere. For example, Fig. 11 illustrates what happens when we fit along the blue wing of the forbidden line instead. We see that now the experimental peak of the allowed line is too high, as is its red wing. Thus by this fitting procedure we have in fact pushed the disagreement into a wavelength range where no disagreement is expected. It suggests that this does not constitute a proper normalization procedure (see also below).

Our previous contention[16] that discrepancies (i) and (ii) are caused by a neglect of ion dynamics has been recently challenged by Lee.[33] He finds that at our densities and temperatures ion dynamic corrections are much too small to explain the observed disagreements. Instead, Lee asserts that a full accounting of the interaction of *all* three upper levels of the atom (the $3\,^1D$, $3\,^1P$, as well as the $3\,^1S$) effectively removes the disagreements

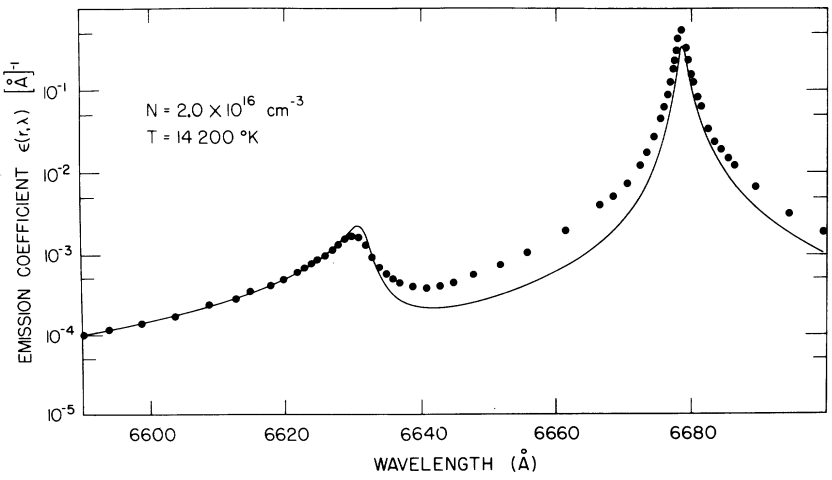

FIG. 11. Same as Fig. 10 except that the normalization factor and continuum level are so chosen as to give the best fit in the vicinity of the forbidden line. Note the discrepancies in the vicinity of the allowed line.

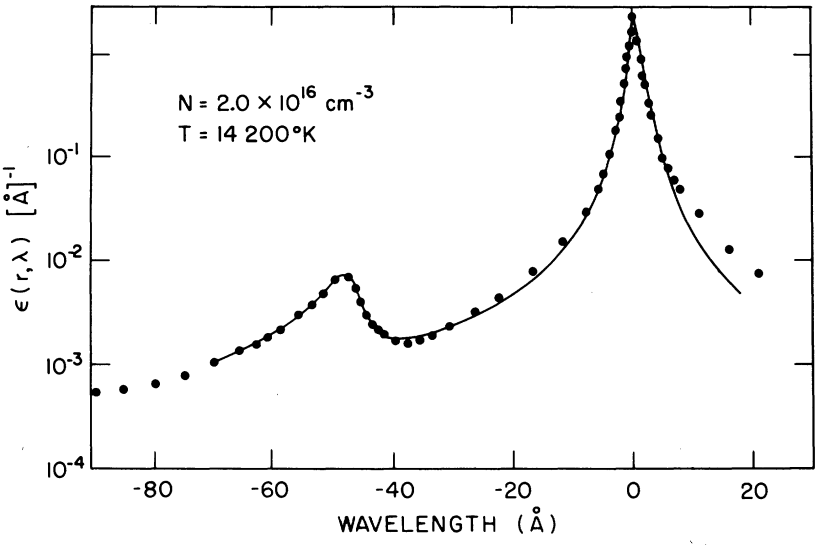

FIG. 12. Profiles of the allowed $2\,^1P$-$3\,^1D$ and the forbidden $2\,^1P$-$3\,^1D$ transition. The dots represent the Abel-inverted experimental profile. The solid line represents the profile computed by Lee (Ref. 33). Note the discrepancies in the red wing of the allowed line.

and he claims to have proved his case by the comparison shown in Fig. 12. Nonetheless, the disagreement along the red wing of the allowed line (apparently similar to that described in Fig. 11), where no disagreements are expected, is disconcerting and remains unexplained. It may well be that here, just as was the case in Fig. 11 the disagreement is in fact along the blue wing of the forbidden line but has been inadvertently moved over by an improper normalization procedure.

IV. CONCLUSIONS

We have examined three forbidden lines of atomic helium. Of these, only one, the He I $2\,^3P$-$4\,^3P$ line at 4517 Å exhibits an agreement with theory which lies well within experimental uncertainties. The line shapes and intensities of the remaining two lines (He I $2\,^3P$-$4\,^3F$ and $2\,^1P$-$3\,^1P$) show some disagreement which are however much less pronounced than has been believed to be the case hitherto. This reduction in the discrepancies is in part due to better line shape measurements, and in part due to recent improvements in the theoretical calculations. The calculations of Deutsch *et al.*[32] for the $2\,^3P$-$4\,^3F$ line show that some of the fine detail around this line is fairly temperature sensitive. This suggests that more accurate determinations of T than those given by us are needed before a definitive evaluation can be made of present-day line shape theories.

ACKNOWLEDGMENTS

The authors wish to thank Dr. C. Deutsch for supplying the theoretical line shapes shown in Fig. 8 and to Dr. Lee for furnishing Fig. 12 prior to publication of his calculation.

*Work supported in part by the U. S. Atomic Energy Commission under Contract No. AT(11-1)-3070.

[1]C. F. Hooper, Jr., Phys. Rev. 165, 215 (1968); Phys. Rev. 149, 77 (1966).
[2]G. Bekefi and C. Deutsch, Comments on Plasma Physics and Controlled Fusion (to be published).
[3]M. A. J. Snijders and A. B. Underhill, Mon. Not. R. Astron. Soc. 151, 215 (1971).
[4]D. S. Leckrone, Thesis (University of California at Los Angeles, 1969) (unpublished).
[5]B. J. O'Mara and R. W. Simpson, Astron. Astrophys. 15, 334 (1971).
[6]G. Bekefi, in *Proceedings of the Tenth International Conference on Phenomenon of Ionized Gases, Oxford, England, September 1971* (Donald Parson & Co., Oxford, England, 1971), p. 299.
[7]H. R. Griem, Astrophys. J. 154, 1111 (1968).
[8]H. A. Gieske and H. R. Griem, Astrophys. J. 157, 963 (1969).
[9]A. J. Barnard, J. Cooper, and L. J. Shamey, Astron. Astrophys. 1, 28 (1969).
[10]A. J. Barnard and J. Cooper, J. Quant. Spectrosc. Radiat. Transfer 10, 695 (1970).
[11]H. R. Griem, *Plasma Spectroscopy* (McGraw-Hill, New York, 1964), Chap. 4.
[12]D. D. Burgess and C. J. Cairns, J. Phys. B 3, L67 (1970); J. Phys. B 4, 1364 (1971).
[13]R. H. Nelson and A. J. Barnard, J. Quant. Spectrosc. Radiat. Transfer 11, 161 (1971).
[14]J. E. Jenkins and D. D. Burgess, J. Phys. B 4, 1353 (1971).
[15]J. W. Birkeland, M. E. Bacon, and W. G. Braun,

Phys. Rev. A 3, 354 (1971).
[16]B. Ya'akobi, E. V. George, G. Bekefi, and R. J. Hawryluk, J. Phys. B 5, 1017 (1972).
[17]G. Bekefi, E. V. George, and B. Ya'akobi, Research Laboratory of Electronics Quarterly Progress Report No. 103, 1971, p. 86 (unpublished); for measurements in lithium plasmas, see B. Ya'akobi, E. V. George, M. Pawlak, and G. Bekefi, in Proceedings of the Fourth European Conference on Controlled Fusion and Plasma Physics, Rome, Italy, August 1970, p. 115 (unpublished).
[18]D. D. Burgess, J. Phys. B 3, L70 (1970).
[19]H. R. Griem, Comments Atom. Molec. Phys. 2, 206 (1971).
[20]R. W. Lee, J. Phys. B 5, L57 (1972); R. W. Lee, J. Phys. B 6, 1044 (1973); R. Grieg, L. A. Jones, and R. W. Lee, Phys. Rev. A (to be published).
[21]E. V. George, G. Bekefi, and B. Ya'akobi, Phys. Fluids 14, 2708 (1971).
[22]W. Lochte-Holtgreven, *Plasma Diagnostics* (North-Holland, Amsterdam, 1968), p. 184.
[23]H. R. Griem, M. Baranger, A. C. Kolb, and G. Oertel, Phys. Rev. 125, 177 (1962).
[24]J. Cooper and G. K. Oertel, Phys. Rev. 180, 286 (1969).
[25]J. R. Greig and L. A. Jones, Phys. Rev. A 1, 1261 (1970).
[26]P. C. Kepple, Phys. Rev. A 6, 1 (1972).
[27]B. Ya'akobi and H. R. Griem (unpublished).
[28]M. C. Richardson and A. J. Alcock, in Proceedings of the European Physical Society Meeting on Laser Interaction with Matter, University of Hull, September 1971, (unpublished).
[29]G. Lampis and S. C. Brown, Phys. Fluids 11, 1137 (1968).
[30]Iu. P. Raizer, Zh. Eksp. Teor. Fiz. 34, 483 (1958) [Sov. Phys.—JETP 34, 331 (1958)].
[31]R. Mewe, Brit. J. Appl. Phys. 18, 107 (1967).
[32]C. Deutsch, C. M. Sassi, and G. Couland, Ann. Phys. (to be published).
[33]R. W. Lee (unpublished).